JCI The Journal of Clinical Investigation

Mosaic analysis of *insulin receptor* function

Tadahiro Kitamura, … , Argiris Efstratiadis, Domenico Accili

J Clin Invest. 2004;113(2):209-219. https://doi.org/10.1172/JCI17810.

Article Endocrinology

Insulin promotes both metabolism and growth. However, it is unclear whether insulin-dependent growth is merely a result of its metabolic actions. Targeted ablation of *insulin receptor* (*Insr*) has not clarified this issue, because of early postnatal lethality. To examine this question, we generated mice with variable cellular mosaicism for null *Insr* alleles. *Insr* ablation in approximately 80% of cells caused extreme growth retardation, lipoatrophy, and hypoglycemia, a clinical constellation that resembles the human syndrome of leprechaunism. *Insr* ablation in 98% of cells, while resulting in similar growth retardation and lipoatrophy, caused diabetes without β-cell hyperplasia. The growth retardation was associated with a greater than 60-fold increase in the expression of hepatic *insulin-like growth factor binding protein-1*. These findings indicate that insulin regulates growth independently of metabolism and that the number of insulin receptors is an important determinant of the specificity of insulin action.

Mosaic analysis of *insulin receptor* function

Tadahiro Kitamura,[1] Yukari Kitamura,[1] Jun Nakae,[1] Antonio Giordano,[2] Saverio Cinti,[2] C. Ronald Kahn,[3] Argiris Efstratiadis,[4] and Domenico Accili[1]

[1]Department of Medicine, College of Physicians & Surgeons of Columbia University, New York, New York, USA
[2]Department of Anatomy, University of Marche, Ancona, Italy
[3]Joslin Diabetes Center, Harvard University, Boston, Massachusetts, USA
[4]Department of Genetics, College of Physicians & Surgeons of Columbia University, New York, New York, USA

Insulin promotes both metabolism and growth. However, it is unclear whether insulin-dependent growth is merely a result of its metabolic actions. Targeted ablation of *insulin receptor* (*Insr*) has not clarified this issue, because of early postnatal lethality. To examine this question, we generated mice with variable cellular mosaicism for null *Insr* alleles. *Insr* ablation in approximately 80% of cells caused extreme growth retardation, lipoatrophy, and hypoglycemia, a clinical constellation that resembles the human syndrome of leprechaunism. *Insr* ablation in 98% of cells, while resulting in similar growth retardation and lipoatrophy, caused diabetes without β-cell hyperplasia. The growth retardation was associated with a greater than 60-fold increase in the expression of hepatic *insulin-like growth factor binding protein-1*. These findings indicate that insulin regulates growth independently of metabolism and that the number of insulin receptors is an important determinant of the specificity of insulin action.

J. Clin. Invest. **113**:209–219 (2004). doi:10.1172/JCI200417810.

Introduction

Insulin regulates fuel utilization and storage, as well as cellular proliferation (1). Despite considerable progress in understanding insulin signaling, it is unclear what engenders the specificity of the biologic response. Among the outstanding questions is whether insulin promotes growth independently of metabolism, or whether the two actions are interdependent (2). We have previously demonstrated that constitutive ablation of the insulin receptor (Insr) results in a mild defect in embryonic growth, attributable to decreased Igf2 signaling (3, 4). In contrast, ablations of *Igf1* and its receptor *Igf1r* result in marked dwarfism at birth (5). These data support a model in which growth and metabolism result from distinct cellular pathways, the former being primarily regulated by Igf signaling and the latter by insulin signaling (6). Moreover, conditional mutagenesis of the Insr is generally devoid of effects on growth, suggesting that insulin does not have growth-promoting effects independent of its metabolic effects (7).

A second, related question is whether, within the same cell type, different insulin responses display different sensitivities to activation of insulin signaling. The issue has profound practical implications because, although defects of insulin action (i.e., insulin resistance) predispose to type 2 diabetes, many of the complications of insulin resistance (e.g., obesity, hypertension, and infertility) appear to arise from excessive rather than decreased insulin signaling. Because insulin acts through a single receptor, the most widely held view is that specific effects arise from signaling elements at a post-receptor level. Extensive tissue-specific mutagenesis of Insr has begun to address these questions, but there are inherent limitations to this approach, since the pattern and extent of tissue recombination is dependent on the specificity of the promoter used to drive Cre expression, which is rarely — if ever — limited to a single tissue or cell type and, even within a given cell type, is generally limited to a specific developmental stage (8). Moreover, it has become apparent that homeostatic mechanisms enable mice to compensate for impaired insulin signaling in a given tissue by shifting substrate utilization to other tissues (9). To circumvent these limitations, we have exploited the powerful genetics of the Cre-*lox*P system to generate mice with variable degrees of cellular mosaicism for null *Insr* alleles (10).

Methods

Reagents. We purchased anti-Insr (C-19) and anti-IGF1 receptor (C-20) antibodies from Santa Cruz Biotech-

Received for publication January 9, 2003, and accepted in revised form November 3, 2003.

Address correspondence to: Domenico Accili, Russ Berrie Medical Science Research Pavilion, 1150 St. Nicholas Avenue, Room 238A, New York, New York 10032, USA.
Phone: (212) 851-5332; Fax: (212) 851-5331;
E-mail: da230@columbia.edu.

Conflict of interest: The authors have declared that no conflict of interest exists.

Nonstandard abbreviations used: *insulin receptor* (*Insr*); *forkhead transcription factor o1* (*Foxo1*); insulin-like growth factor binding protein-1 (Igfbp1); phosphatidylinositol-tris-phosphate (PIP3); pancreatic and duodenal homeobox protein-1 (Pdx1); peroxisome proliferative activated receptor, γ, coactivator 1α (Pgc1α); heat shock promoter (HSP); HSP 70-1 Cre transgenic (*Hs-Cre6*); growth hormone (GH); triglyceride (TG); ^{125}I-labeled insulin (^{125}I-insulin); ^{125}I-labeled IGF2 (^{125}I-IGF2); brown adipose tissue (BAT); *phosphoenol-pyruvate carboxykinase* (*Pck1*); *glucose-6-phosphatase* (*G6pc*); *hepatic glucose transporter Glut2* (*Slc2a2*); *glucokinase* (*Gck*); *sterol regulatory element binding transcription factor-1* (*Srebf1*); *glycogen synthase* (*Gys1*); *glycogen phosphorylase* (*Pygl*); *phosphofructokinase, liver* (*Pfkl*); *forkhead transcription factor a2* (*Foxa2*); *uncoupling protein-1* (*Ucp1*); *peroxisome proliferator activator receptor γ* (*Pparγ*); *adrenergic β$_3$ receptor* (*Adrb3*).

nology Inc. (Santa Cruz, California, USA), anti-insulin and anti-glucagon antisera from Linco Research Inc. (St. Charles, Missouri, USA), anti-*forkhead transcription factor o1* (anti-*Foxo1*) and anti-phosphoS253 *Foxo1* from Cell Signaling Technology Inc. (Beverly, Massachusetts, USA), anti-dynamin, anti–insulin-like growth factor binding protein-1 (anti-Igfbp1), anti-Igfbp2, and anti-Igfbp4 from Upstate Biotechnology Inc. (Lake Placid, New York, USA), anti–phosphatidylinositol-tris-phosphate (anti-PIP3) from Echelon Research Laboratories Inc. (Salt Lake City, Utah, USA). We obtained the anti–pancreatic and duodenal homeobox gene-1 (anti-Pdx1) antiserum from C. Wright (Vanderbilt University, Nashville, Tennessee, USA) and the anti–peroxisome proliferative activated receptor, γ, coactivator 1α (anti-Pgc1α) antiserum from B. Spiegelman (Harvard University, Cambridge, Massachusetts, USA).

Animal production and phenotypic analysis. The Columbia University Institutional Animal Care and Utilization Committee have approved all animal procedures (Protocol no. 2715-3). We have described previously the generation of $Insr^{flox}$ (11) mice, in which exon 4 of Insr is flanked by loxP sites, and heat shock promoter (HSP 70-1) Cre transgenic (*Hs-Cre6*) mice (10). To generate Insr mosaics, we intercrossed $Insr^{lox/lox}$ and *Hs-Cre6* mice to obtain $Insr^{lox/lox,\ Hs\text{-}Cre}$ hemizygous mice. These were then backcrossed with $Insr^{lox/lox}$ mice to obtain mosaics. Thus, in the ensuing progeny, the *Hs-Cre* transgene was always hemizygous. In the initial set of experiments, we genotyped the resulting progeny by RT-PCR of tail RNA, carried out as described below and exemplified in Figure 1, a and b. However, in subsequent experiments, we assigned individual mice to either the Δ80 or Δ98 categories post hoc, based on the levels of Insr protein detected on a liver Western blot performed after sacrificing the animals. We carried out metabolic analyses as described previously (12), and measured immunoreactive growth hormone (GH) (Linco Research Inc.) and IGF1 (Diagnostic Systems Laboratories Inc., Webster, Texas, USA) using RIA kits. We performed growth analysis as described (13). We measured tissue glycogen content as described previously (14). We measured triglycerides (TGs) with the Trig GB kit (Roche Diagnostics, Basel, Switzerland) and FFA with the NEFA C Test kit (Wako Chemicals USA Inc., Richmond, Virginia, USA).

Western blotting, insulin binding, and ligand blot assays. For Western blotting, we homogenized tissues (50 mg) in buffer containing 20 mM Tris (pH 7.5), 10 mM EGTA, 10 mM $MgCl_2$, 1% NP-40, 1 mM PMSF, 1 mM DTT. We clarified the lysate by centrifugation at 10,000 *g* for 30 minutes at 4°C, and resolved proteins on SDS-PAGE.

We carried out ^{125}I-labeled insulin (^{125}I-insulin) binding as described (15). We expressed binding as a percentage of WT values, after subtraction of nonspecific binding. We used tissues from *Insr* KO mice as controls. For ^{125}I-labeled IGF2 (^{125}I-IGF2) ligand blot assays, we used the protocol described by Ooi et al. (16) and used 5 ml of serum. In some experiments, serum was immunoprecipitated with anti-Igfbp1, anti-Igfbp2, or anti-Igfbp4 antisera prior to gel electrophoresis and transfer to nylon membranes.

Histologic analysis. We removed brown adipose tissue (BAT), livers, and pancreata from WT, Δ80, and Δ98 mice, fixed and embedded them in paraffin, and mounted consecutive 5- to 10-μm sections on slides. For adipose tissue and liver, we stained sections with H&E. We immunostained pancreata for β and α cells using anti-insulin and anti-glucagon antibodies, respectively. For immunofluorescence with anti-Pdx1 and anti-Foxo1 antibodies, we prepared frozen pancreas sections. We used anti-Pdx1 and anti-Foxo1 antibodies at dilutions of 1:5,000 and 1:30, respectively. We used FITC-conjugated secondary anti-rabbit IgG to visualize the immune complexes.

Light microscopy and EM. We fixed small tissue fragments in 2% glutaraldehyde and 2% paraformaldehyde in 0.1 M phosphate buffer (pH 7.4), postfixed in 1% OsO_4, dehydrated them in ethanol, and embedded them in an Epon–Araldite mixture (Epon: Multilab Supplies, Fetcham, United Kingdom; Araldite: Fluka Chemie, Buchs, Switzerland). Semithin sections (2 μm) were stained with toluidine blue O; thin sections were obtained with a MT-X ultratome (RMC, Tucson, Arizona, USA), stained with lead citrate, and examined with a Philips CM10 transmission electron microscope (Royal Philips Electronics, Eindhoven, The Netherlands).

PIP3 immunohistochemistry. Mice were anesthetized with pentobarbital, and insulin (1 mU) or normal saline was administered via the portal vein, followed 3 minutes later by perfusion with 4% paraformaldehyde in 0.1 M phosphate buffer (pH 7.4). Liver samples were removed and fixed overnight in 4% paraformaldehyde, followed by 25% sucrose overnight at 4°C. They were snap-frozen in OCT Compound (Sakura Finetechnical Co., Tokyo, Japan) and sectioned using a cryostat to yield 7-μm-thick sections. Liver sections were equilibrated in PBS at room temperature after blocking with 5% goat serum and 2% bovine serum in PBS, and were then incubated with mouse anti-PIP3 antibody (Echelon) at a 1:100 dilution overnight at 4°C. The antibody was detected with cyanin-3-conjugated goat anti-mouse antibody at a 1:200 dilution (Jackson Immunoresearch Laboratories Inc., West Grove, Pennsylvania, USA). After washing with PBS, the sections were counterstained with DAPI (Molecular Probes Inc., Eugene, Oregon, USA) to identify the nucleus.

Immunohistochemical and morphometric analyses. Pancreata were removed from 3-week-old mice, weighed, and fixed overnight in 4% paraformaldehyde. Sections (4 μm thick) were immunostained for β cells using mouse anti-insulin antibodies and for α cells using mouse anti-glucagon antibodies (Sigma-Aldrich, St. Louis, Missouri, USA). For morphometric analysis of β-cell mass, three animals of each genotype were analyzed. For each pancreas, three sections spaced at least 40 μm (Δ80 and Δ98 mice) and 160 μm apart (WT mice) were covered systematically by accumulating images from nonoverlapping fields that were captured

with a digital camera (Nikon 950; Nikon Inc., Melville, New York, USA) and analyzed using the NIH Image 1.60 software, as described (17). Results were expressed as a percentage of the total surveyed pancreatic area occupied by α and β cells. β-cell mass was calculated by multiplying β-cell area by pancreatic weight.

Real-time RT-PCR and Northern blot analysis. We isolated mRNA from liver tissue and BAT using the MicroFast Track 2.0 kit (Invitrogen Corp., San Diego, California, USA). We performed Northern blot analysis according to standard methods. For semiquantitative RT-PCR analysis to evaluate the efficiency for excision of the "floxed" *Insr*, we used a set of primers located in Insr exon 3 (5′-CTGTTCGGAACCTGATGA-3′) and exon 5 (5′-GTGATACCAGAGGATAGGAG-3′). We performed real-time RT-PCR using primer sets encoding *Igfbp1*, *phosphoenol-pyruvate carboxykinase* (*Pck1*), *glucose-6-phosphatase* (*G6pc*), *hepatic glucose transporter Glut2* (*Slc2a2*), *glucokinase* (*Gck*), *sterol regulatory element binding transcription factor 1* (*Srebf1*), *glycogen synthase* (*Gys1*), *glycogen phosphorylase* (*Pygl*), *phosphofructokinase, liver* (*Pfkl*), *Foxo1*, *forkhead transcription factor-a2* (*Foxa2*), *uncoupling protein-1* (*Ucp1*), *peroxisome proliferator activator receptor γ* (*Pparγ*), *Pgc1α*, and *adrenergic β3 receptor* (*Adrb3*). Primer sequences are available upon request. For these experiments, we isolated mRNA from more than eight mice for each genotype and amplified mRNA from each mouse individually using a Roche Light Cycler PCR instrument and Light Cycler RT-PCR kit (Roche Perkin-Elmer, Foster City, California, USA). We carried out each reaction in triplicate, using a standard curve with the relevant cDNA for each primer set.

Results

Generation of Insr mosaics. To generate mice with variable degrees of *Insr* inactivation, we used a binary system based on Cre-*loxP* recombination. We have previously shown that mice expressing the Cre recombinase under transcriptional control of the HSP 70-1 promoter (*Hs-Cre6*) can be used for mosaic analysis of mice carrying floxed alleles (10). In *Hs-Cre6* mice, a transient activation of Cre expression occurs in a stochastic manner in the two-cell embryo (10), yielding progeny with cellular mosaicism for gene deletions, when these transgenics are crossed with responder floxed mice. In the offspring, every tissue will be composed of an admixture of cells carrying either intact or null alleles of the gene of interest. Because Cre acts catalytically (18), the likelihood of obtaining heterozygous cells carrying a combination of intact and deleted alleles is, for all intents and purposes, negligible. We have shown that the degree of mosaicism varies between 0% and 100% (10).

We crossed mice bearing a floxed *Insr* allele (11) with *Hs-Cre6* transgenics (10). The resulting $Insr^{lox/+}$*Hs-Cre6* mice were backcrossed with $Insr^{lox/lox}$ mice to obtain $Insr^{lox/lox}$*Hs-Cre6* mice. These mice displayed different degrees of cellular mosaicism for null alleles of *Insr*, ranging between less than 5% and greater than 98%. We measured the degree of *Insr* inactivation by an RT-PCR assay on liver mRNA that amplified both a 500-bp product derived from the WT *Insr* allele and a 350-bp product, derived from the deleted allele (Figure 1a). We confirmed the extent of depletion of the protein product by immunoblotting with anti-Insr antiserum (Figure 1b). As a control, IGF1 receptor (Igf1r) levels were unchanged (Figure 1b). To increase the frequency of the desired $Insr^{lox/lox}$*Hs-Cre6* phenotype, we intercrossed $Insr^{lox/lox}$*Hs-Cre6* mice with a low degree of mosaicism (less than 5%) with $Insr^{lox/lox}$ mice to generate mosaics carrying the transgene in the hemizygous state. Among offspring from these crosses, we selected two subsets of mosaic mice for further analysis: the first subset had an approximately 80% reduction of Insr levels (thereafter referred to as Δ80) (Figure 1a, lane 2). A second subset had an approximately 98% reduction of Insr levels (thereafter referred to as Δ98) (Figure 1a, lane 5). The reduction of Insr protein levels in different tissues within each subset of mice was similar, with brain tissue

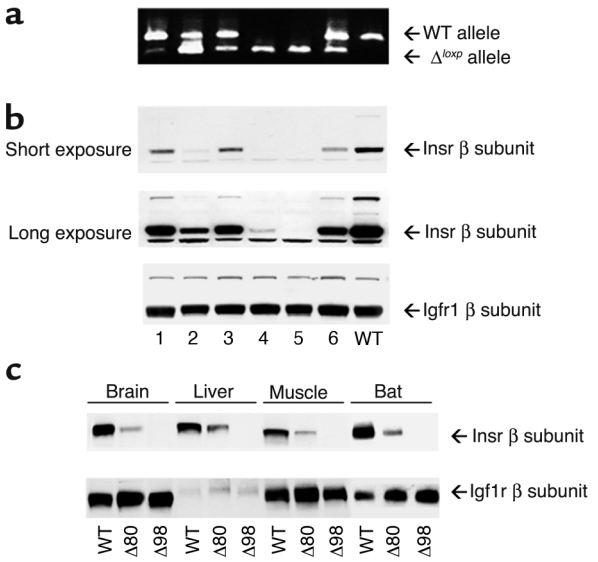

Figure 1
Evaluation of *Insr* mosaicism. (**a**) RT-PCR analysis. We isolated mRNA from liver of individual mosaic (lanes 1–6) and WT (lane 7) mice. Because of the deletion of *Insr* exon 4, the length of the PCR product generated from the Δ^{loxP} allele is smaller (350 bp) than the WT allele (500 bp) (upper panel). (**b**) Protein levels of Insr and Igf1r were examined by Western blotting as indicated in Methods. The first and second panels from the top show different exposures of the same autoradiogram to better visualize Insr expression in mice with greater degrees of mosaicism. The third panel from the top shows samples from the same set of mice analyzed with anti-Igf1r antiserum to normalize protein levels. (**c**) Expression level of Insr in various tissues in Δ80 and Δ98 mice by Western blotting. We removed brain, liver, skeletal muscle, and BAT and determined protein levels of Insr and Igf1r by Western blotting as indicated in Methods.

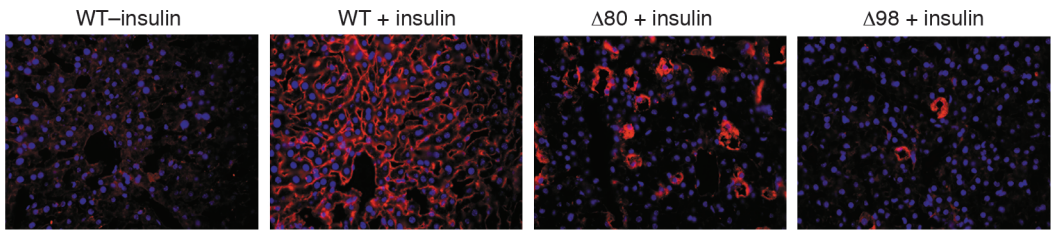

Figure 2
In vivo generation of PIP3 in response to insulin. We injected insulin via the inferior vena cava of anesthetized mice and after 3 minutes perfused the liver with paraformaldehyde. We then processed the livers for histochemistry with anti-PIP3 antiserum as described. We applied nuclear counterstain to count cell number. We analyzed multiple sections from three mice for each genotype. A representative experiment is shown.

showing the most extensive depletion, muscle tissue and BAT showing intermediate levels, and liver tissue showing the least extensive Insr depletion (Figure 1c). We confirmed the extent of Insr ablation by ^{125}I-insulin binding to extracts from various tissues (Table 1). These findings are consistent with previously reported tissue patterns of *Hs-Cre*–mediated recombination at several additional floxed loci (10).

Demonstration of mosaicism. To assess the extent of mosaicism in vivo, we injected insulin via the portal vein and visualized the generation of PIP3 in the liver by a histochemical method. In WT mice, insulin induced generation of PIP3 and its juxta-membrane localization. In Δ80 mice, the number of PIP3$^+$ cells was about 20%; in Δ98 mice the number was about 2% of the total (Figure 2). Thus, the degree of genetic mosaicism correlates with the decrease in Insr protein levels and with a decrease in the number of cells in which insulin signaling leads to PIP3 generation. These data indicate that tissues of mosaic mice consist of an admixture of WT and null cells, with few if any cells carrying the *Insr* heterozygous deletion (see Methods). The data are also consistent with the lack of cell-autonomous actions of insulin, at least within the experimental limits of this approach, since there does not appear to be activation of insulin signaling in a greater percentage of cells than expected based on the levels of DNA mosaicism.

Growth retardation and lipoatrophy are common features of Δ80 and Δ98 mice. Offspring from both subsets had a normal appearance and weight at birth. However, they failed to thrive thereafter, and attained approximately 30% of normal weight at 3 weeks (Figure 3, a and b). The majority of animals died at weaning (about 3 weeks after birth), when insulin requirements increase (19). While none of the Δ80 mice survived longer than 3 weeks, about 5% of Δ98 mice survived as long as 3 months. However, their growth was persistently stunted, and they reached about 20% of normal weight at that age (Figure 3c). Circulating GH levels in 14-day-old mice were normal, whereas IGF1 levels showed a twofold increase in both subsets ($P < 0.05$ by ANOVA) (Table 2). We detected a greater than 60-fold increase in *Igfbp1* mRNA levels by real-time-PCR and Northern blotting (Figure 3, d and e). Serum ligand blotting with ^{125}I-IGF2 confirmed the increase in Igfbp1, and showed normal levels of Igfbp2 (Figure 3f) and Igfbp3 (not shown). The extent of growth retardation in Δ98 survivors is similar to that observed in mice with combined mutations of *Ghr* and *Igf1*, which ablate both GH-dependent and GH-independent IGF functions and achieve about 17% of normal weight (20). However, unlike IGF1-deficient mice, which display both intrauterine and postnatal growth retardation (21), Δ80 and Δ98 mice are born of normal size.

Necroscopic and histologic analyses revealed the complete absence of mature adipocytes in the interscapular (BAT), subcutaneous, and epididymal (white adipose tissue, EWAT) regions of both subsets of mice. To simplify presentation, only data on Δ98 mice are shown (Figure 4a), but we obtained identical data in Δ80 mice. To ascertain whether the absence of adipocytes was due to impaired pre-adipocyte differentiation or increased lipolysis, we analyzed both areas by EM. Wild-type EWAT consisted of well-developed adipocytes with a single lipid droplet in the cytoplasm. In contrast, EWAT derived from Δ80 and Δ98 mice had a fetal/perinatal appearance, with abundant WAT precursors, without evidence of de-lipidated mature adipocytes (22). A peculiar EM finding was the presence of enlarged mitochondria with large electron-dense inclusions (Figure 4, b–d). The nature of these formations is unclear, but they may be related to development of the chondriome (22). Similarly, brown adipocytes in mosaic mice appeared similar to fetal BAT pre-adipocytes (Figure 4, e and f). Although the distinction between pre-adipocytes and de-lipidated mature adipocytes is less well established in BAT than in EWAT, the presence of immature mitochondria with unorganized cristae (Figure 4f) and the lack of tannic acid–reactive material (not shown) are consistent with

Table 1
^{125}I-insulin binding

Genotype	Δ80	Δ98
Liver	24.7 ± 1.9	2.9 ± 0.9
Brain	8.1 ± 0.9	1.9 ± 0.6
Muscle	19.7 ± 1.8	2.5 ± 1.1
Brown adipocytes	15.6 ± 1.3	2.1 ± 0.3

Quantitation of Insr levels by insulin binding. Numbers represent mean ± SEM of at least 12 mice for each genotype, expressed as the percentage of binding to extracts from WT mice.

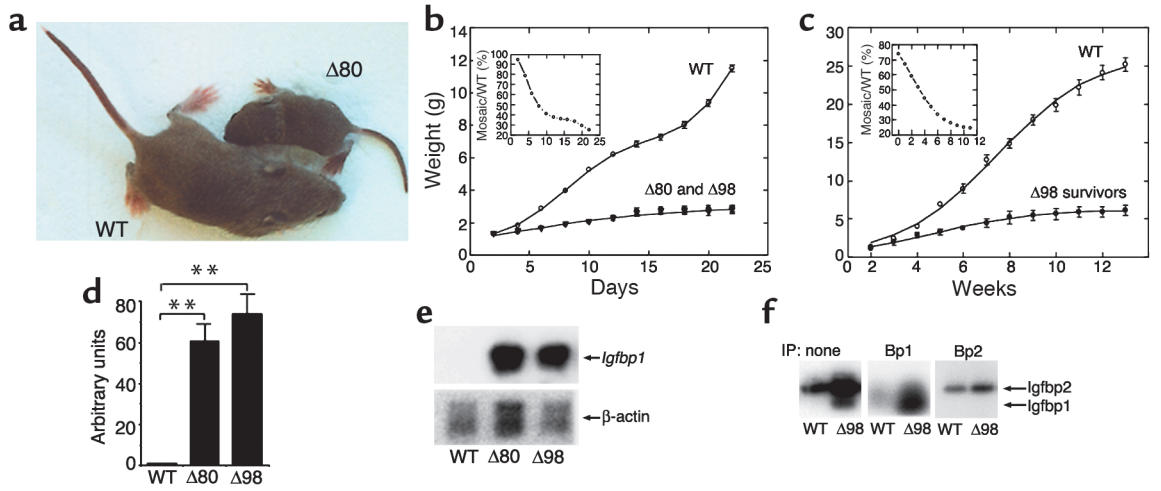

Figure 3

Growth retardation in Insr mosaics. (**a**) Appearance of 3-week-old mice. (**b**) Average growth curves of WT and mosaic mice. The curves of the two subsets of mosaics are superimposable. The analysis was terminated at the time of death of Δ80 mosaics (n = 19 for WT, 18 for Δ80, and 15 for Δ98). (**c**) Δ98 survivors were followed for up to 13 weeks. The data represent the mean ± SEM (n = 28 for WT and 19 for Δ98 survivors). The insets present weight ratios of mosaic mice to WT control per time point examined. The decline of these ratios is indicative of lower than normal growth rate for the mosaics throughout the period of observation. (**d**) Real-time RT-PCR analysis of *Igfbp1* expression in liver. We isolated total RNA from WT (n = 20), Δ80 (n = 17), and Δ98 (n = 20) mice and subjected it to RT-PCR using a Light Cycler instrument (Roche Perkin-Elmer). We normalized mRNA values using β-actin as a control. $^{**}P < 0.01$. (**e**) Northern blot analysis of *Igfbp1* expression. We pooled mRNA samples from four different mice for each set and analyzed them by hybridization with an *Igfbp1* probe (upper panel), followed by a β-actin probe as gel loading control. (**f**) ^{125}I-IGF2 ligand blotting. We obtained serum (5 μl for each animal) from WT (n = 10) and Δ98 mice (n = 10). In the panel on the left, we used whole serum to determine the presence of IGF-binding proteins. As shown, in the middle and right panels, we subjected serum to immunoprecipitation (IP) with the indicated antibodies (Bp1, Bp2) prior to gel electrophoresis and transfer to nylon membranes. We show the region of the gel in the 20- to 40-kDa region.

the notion that these are undifferentiated pre-adipocytes (22). In addition, we analyzed expression of key genes in BAT function, including *Adrb3*, *Ucp1*, *Pparγ* and its co-activator *Pgc1α*. *Ucp1* expression decreased by about 95%, *Pparγ* by 80%, and *Pgc1α* by 60% in both subsets (Figure 4g). Since insulin regulates Pgc1α by both transcriptional and translational mechanisms (23), we also examined Pgc1α protein levels. Immunoblotting confirmed the decrease in Pgc1α levels (Figure 4g, lower panels). mRNA levels of *Adrb3*, a known inducer of *Ucp1* expression, were normal in both lines (Figure 4g). These data indicate that lipoatrophy is due to impaired adipocyte differentiation, rather than increased lipolysis.

Hypoglycemia versus hyperglycemia in Δ80 and Δ98 mice. We examined several metabolic parameters (Table 2). Δ80 mice exhibited hypoglycemia associated with an approximately threefold increase in insulin levels. Although the cause of death for both groups of mice is unclear, hypoglycemia is a probable contributor in Δ80 mice. FFA levels were normal, whereas TG levels were reduced by about 50%. Hepatic glycogen levels were severely reduced, while muscle glycogen levels were normal. Since mobilization of hepatic glycogen is required to maintain euglycemia during fasting, it is likely that hypoglycemia in Δ80 mice results from reduced hepatic glycogen content. The hypoglycemia observed in this subset of mice is reminiscent of that seen in the human syndrome of leprechaunism, caused by *INSR* mutations (24).

In contrast to Δ80 mice, Δ98 mice exhibited hyperglycemia and an approximately 13-fold increase in insulin levels. This metabolic condition is similar to that observed in Insr KO mice (3). As in Δ80 mice, hepatic glycogen content was severely decreased. Unlike Δ80 mice, Δ98 mice also showed a greater than 80% decrease in muscle glycogen content (Table 2).

The difference in glucose levels between Δ80 and Δ98 mice is noteworthy and could potentially be explained by altered expression of genes involved in hepatic glucose handling. For example, it might have been predicted that hypoglycemic Δ80 mice had reduced levels of glucogenic enzymes, while hyperglycemic Δ98 had high levels. Real-time RT-PCR analysis showed that this is not the case (Figure 5a). In fact, *Pck1* increased three- to fivefold and *G6pc* was unchanged in both subsets. The only difference was in *Pfkl* levels, which were significantly elevated only in Δ98 mice but are by themselves unlikely to explain the phenotype. *Gys1* and *Pygl* decreased in both Δ80 and Δ98 mice. Since these enzymes are important for glycogen synthesis and release, the combined decrease in synthase and phosphorylase cannot explain the decrease in glycogen content. *Glut2* (*Slc2a2*) showed an approximately 40% decrease exclusively in Δ80 mice, while *Gck* levels were unchanged. However, given that even a complete ablation of Glut2 does not affect hepatic glucose output (25), the observed decrease in Δ80 mice is unlikely to represent the sole cause of the difference in glucose levels between the two subsets.

Table 2
Metabolic parameters in Insr mosaics

Genotype	*n*	WT	Δ80	Δ98
Glucose (mg/dl)	40	102 ± 8	47 ± 6	258 ± 16
Insulin (ng/ml)	40	0.30 ± 0.04	0.92 ± 0.21	4.0 ± 0.9
β-cell mass (μg/pancreas)	3	510 ± 28	128 ± 17	144 ± 25
IGF1 (ng/ml)	40	430 ± 49.7	819 ± 52.3	891 ± 69.2
GH (ng/ml)	40	1.38 ± 0.33	0.98 ± 0.22	1.25 ± 0.30
FFA (mEq/l)	20	0.81 ± 0.13	0.78 ± 0.11	0.82 ± 0.12
TG (mg/dl)	20	56 ± 2	27 ± 5	23 ± 4
Hepatic glycogen (mg/g)	20	14.2 ± 2.7	2.7 ± 1.0	0.08 ± 0.01
Muscle glycogen (mg/g)	20	1.42 ± 0.04	1.26 ± 0.21	0.26 ± 0.05

Overexpression of *Foxa2* in the liver of transgenic mice results in postnatal growth retardation, elevated Igfbp1, and reduced hepatic glycogen content (26). To address the possibility that the observed phenotype could be due to altered *Foxa2* expression, we measured its mRNA levels. In both subsets of mice, *Foxa2* was decreased, thus ruling out its involvement in this phenotype. On the other hand, the forkhead transcription factor Foxo1 promotes *Pck1*, *G6pc*, and *Igfbp1* expression, and is inhibited by insulin via Akt-mediated phosphorylation (14). *Foxo1* mRNA (not shown) and protein levels were normal in both subsets, but the phosphate content of the key Akt phosphorylation site was decreased by about 40% and 60% in Δ80 and Δ98 mice, respectively, consistent with increased transcriptional activity (Figure 5b). Thus, the increase in glycogen mobilization can be explained in part by unrestrained Foxo1 activity. Among the Foxo1 targets, the transcriptional co-activator *Pgc1α* (27) was increased by twofold and fourfold in Δ80 and Δ98 mice, respectively (Figure 5a). Pgc1α cooperates with Foxo1 to increase *Pck1* and *G6pc* transcription (7), and the observed increase is likely to represent a compensatory response to increase gluconeogenesis, as observed with prolonged fasting (28). To summarize these data, both Δ80 and Δ98 mice had similar alterations of hepatic gene expression and glycogen content. Thus, the difference in circulating glucose levels cannot be explained by liver metabolism.

We next analyzed insulin signaling in muscle extracts from the two sets of mosaics. In Δ80 mice, insulin-dependent co-precipitation of the p85 subunit of PI3K with anti-phosphotyrosine antiserum was reduced by about 80%, as was the amount of phospho-Akt. In Δ98 mice, there was a greater than 90% decrease in p85 co-precipitation, while no phospho-Akt could be detected in response to insulin (Figure 6). Thus, muscle insulin signaling is decreased in proportion to the degree of *Insr* mosaicism.

The small size of these mice preempts further metabolic analyses. Nevertheless, based on these observations, we suggest the following model for the difference in glucose levels between Δ80 and Δ98 mice. In the liver, both groups of mice are equally insulin-resistant, as demonstrated by the comparable expression of metabolic control genes and glycogen levels. Hepatic insulin resistance causes inability to synthesize and store glycogen; this explains the fasting hypoglycemia in Δ80 mice. In contrast to liver, biochemical data indicate that residual insulin signaling is present in Δ80 mice but not in Δ98 mice, as demonstrated by phospho-Akt levels. Consistent with this observation, muscle glycogen content is normal in Δ80 mice but reduced in Δ98 mice. These data indicate that Δ80 mice are insulin-sensitive in the muscle, whereas Δ98 are insulin-resistant. Sensitivity to insulin in the muscle would be expected to exacerbate hypoglycemia in Δ80 mice, because glucose is cleared from the blood and taken up by skeletal muscle. In contrast, resistance to insulin action in the muscle of Δ98 mice results in impaired glucose uptake and hyperglycemia. In summary, we propose that the difference between the two strains is due to tissue-specific differences in insulin resistance. While in theory

Table 3
Phenotypic comparison between Insr mosaics and leprechaunism

	Leprechaunism	Δ80	Δ98	Insr KO
Growth	Prenatal and postnatal retardation	Postnatal retardation	Postnatal retardation	Near normal (90%)
Life span	<1 year	3 weeks	3 weeks (95%), 3 months (5%)	<1 week
Glucose	Low	Low	High	High
Insulin	High (up to 1,000-fold)	High (one- to threefold)	High (2- to 20-fold)	High (5- to 50-fold)
Ketoacidosis	Transient	Absent	Constant	Constant
Hepatic steatosis	Moderate	Moderate	Severe	Severe
Lipoatrophy	Present	Present	Present	Present

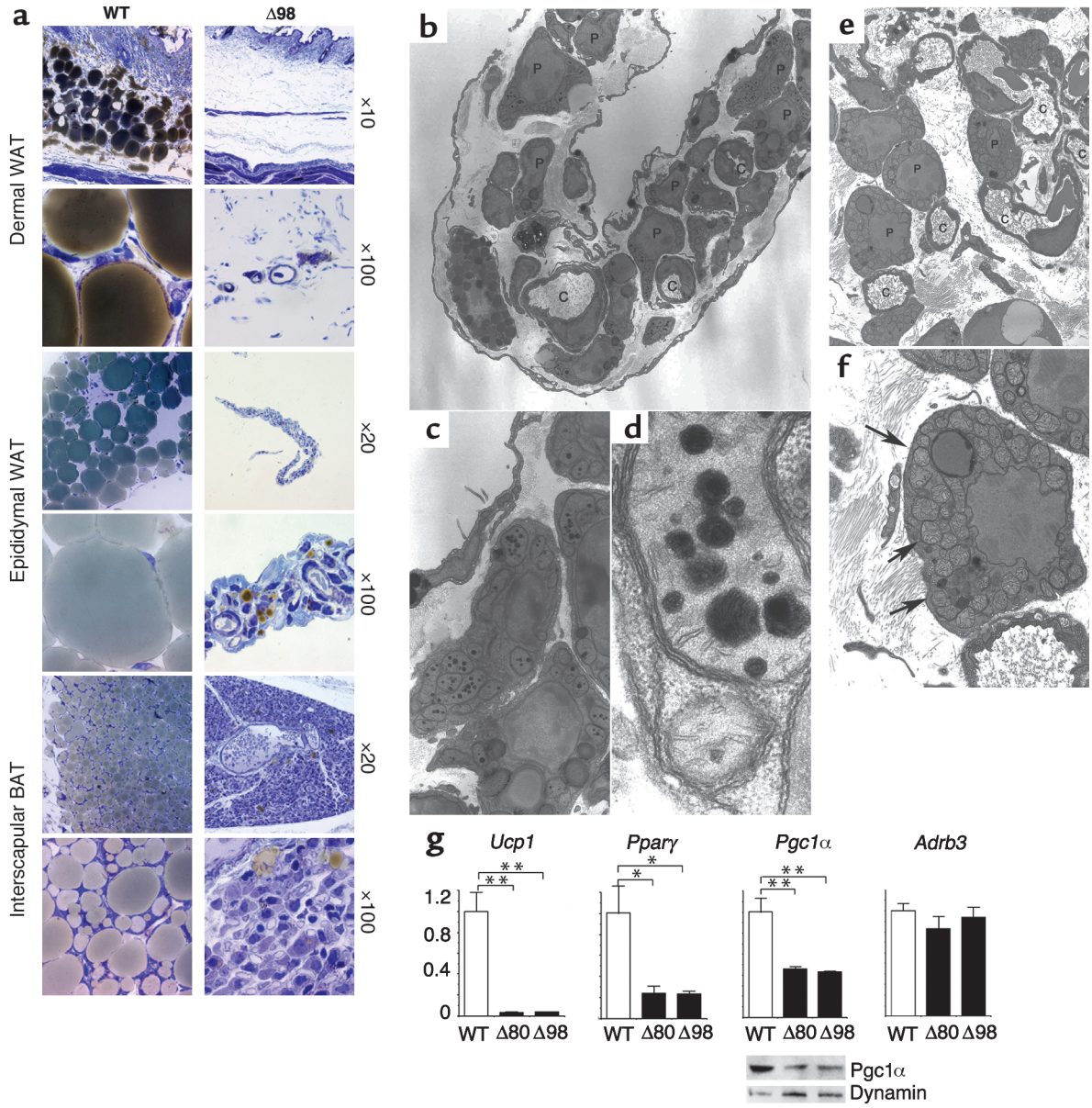

Figure 4
Lipoatrophy and analysis of BAT gene expression. (**a**) Representative histologic appearance of H&E-stained sections from dermal WAT, peri-epididymal WAT, and BAT. For simplicity, only Δ98 mice are shown, but the data are identical in Δ80 mice. (**b**–**d**) EM analysis of peri-epididymal WAT precursors in Δ98 mice. The magnifications shown are (**b**) ×1,900, (**c**) ×5,000, and (**d**) ×46,000. Intramitochondrial inclusions of electron-dense material are shown in **b** and **d**. The mitochondria are enlarged and show poorly organized cristae. (**e** and **f**) EM analysis of BAT precursors in Δ98 mice. Numerous pre-adipocytes adjacent to small capillaries can be seen. Mitochondria are indicated by arrows. The magnifications shown are (**e**) ×1,900 and (**f**) ×5,000. P, pre-adipocytes; C, capillaries; L, lipid droplet. (**g**) Analysis of BAT gene expression. We isolated mRNA from 3-week-old mice and performed real-time RT-PCR with primers encoding the genes indicated at the top of each panel. The data represent means ± SEM of three independent measurements (n = 10 for each genotype). We used amplification of β-actin to normalize gene expression data. Asterisks indicate a statistically significant difference (*P < 0.05 and **P < 0.01 by ANOVA) between genotypes. To measure the levels of immunoreactive Pgc1α, we performed Western blotting with anti-Pgc1α antiserum. We show a representative autoradiogram and a loading control with anti-dynamin antiserum below the Pgc1α real-time PCR graph.

the difference could be due to variations in the counter-regulatory response between the two sets of mice, the presence of normal GH levels and the normal glucagon histochemistry (Figure 7) make that interpretation less likely.

Lipoatrophy without dyslipidemia in Δ80 and Δ98 mice. Lipoatrophy is generally associated with severe hyperinsulinemia, hepatic steatosis, and increased FFA and TG levels (29, 30). However, fatty liver infiltration was absent in Δ80 mice and modest in Δ98 mice (Figure 5c). Moreover, FFA and TG levels were normal or low in both subsets, and insulin levels were only moderately elevated in Δ98 mice (Table 2). To determine the mechanism of this

dissociation between lipoatrophy and lipid abnormalities, we measured expression of the transcription factor *Srebf1*, which regulates expression of lipogenic (31) and gluconeogenetic (32) genes in an insulin-dependent manner (33). In both subsets, we found a substantial decrease in *Srebf1* expression (Figure 5a), suggesting that the lack of hyperlipidemia in *Insr* mosaics is due to reduced Srebf1-mediated lipid synthesis.

Lack of compensatory β-cell hyperplasia in Δ98 mice. We next examined pancreatic histomorphometry in both lines. We could not recover islets from Δ80 or Δ98 mice to measure the degree of *Insr* mosaicism, because of their small size. Nevertheless, given the common endodermal derivation of liver and pancreas (34), it is fair to assume that the degree of cellular mosaicism in pancreatic islets mirrored that seen in liver tissue. Despite the mild-to-moderate increases in insulin levels, islet size and morphology in mosaic animals were similar to those in WT mice (Figure 7), and β-cell mass was proportional to pancreas size (Table 1). Thus, given the hyperglycemia in Δ98 mice, β-cell mass should be considered inappropriately small. Indeed, the number of β cells with nuclear expression of the insulin gene transcription factor Pdx1 decreased in approximate proportion to the degree of *Insr* mosaicism. Interestingly, in islets of Δ98 mice, Pdx1 often mislocalized to the cytoplasm, but the significance of this observation is controversial (35). We recently reported that Foxo1 regulates *Pdx1* expression in pancreatic β cells (36). Whereas Foxo1 showed variable subcellular distribution in WT β cells, it showed exclusive nuclear localization in β cells from Δ98 mice (Figure 7). These data can be interpreted to suggest that the probable impairment of insulin signaling in β cells prevents β-cell compensation to insulin resistance, without affecting fetal β-cell development and their postnatal secretory function.

Discussion

We draw two main conclusions from our mosaic analysis of Insr function. First, different biological responses to insulin appear to have different sensitivities to reduction of Insr signaling. Thus, it appears that insulin-dependent growth, adipogenesis, and hepatic glycogen synthesis are more sensitive to depletion of Insr than muscle glycogen synthesis, which in turn probably reflects decreased insulin-dependent glucose uptake. Second, despite the profound depletion of Insr, mosaic mice developed few if any of the metabolic consequences of insulin resistance, such as β-cell hyperplasia, obesity, and dyslipidemia.

Studies of insulin-induced PIP3 generation in mosaic mice show a close correlation between the number of

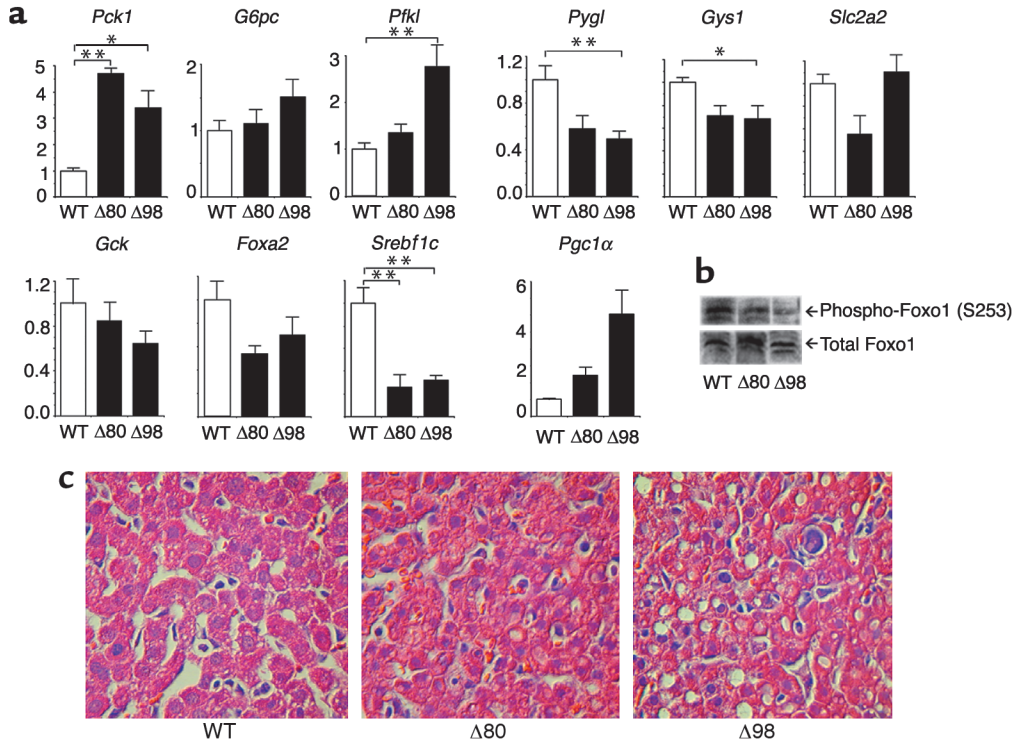

Figure 5

Analysis of liver gene expression, Foxo1 phosphorylation, and histology. (**a**) Real-time RT-PCR. We isolated mRNA from the liver of 3-week-old mice and performed real-time RT-PCR with primers encoding the genes indicated at the top of each bar graph. The data represent means ± SEM of three independent measurements ($n = 14$ for each genotype). *$P < 0.05$. **$P < 0.01$. (**b**) Foxo1 phosphorylation. We removed the livers from WT, Δ80, and Δ98 mice and isolated proteins by detergent extraction. We performed Western blotting with anti-phospho S253 Foxo1 antibody (upper panel), and then probed the filter again with anti-Foxo1 antibody (lower panel). We show a representative experiment. (**c**) H&E-stained liver sections from WT, Δ80, and Δ98 mice.

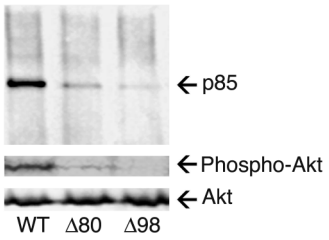

Figure 6
Muscle insulin signaling. Mice were treated with insulin, delivered via the inferior vena cava, and protein extracts were prepared and analyzed by immunoprecipitation with anti-phosphotyrosine antiserum followed by immunoblotting with anti-p85 antiserum (upper panel). Alternatively, extracts were resolved on SDS-PAGE and analyzed by immunoblotting with anti-pSer^{473}-Akt antiserum (middle panel), followed by reprobing of the stripped blots with anti-Akt antiserum (bottom panel).

PIP3$^+$ cells and the degree of mosaicism. While technical limitations prevent us from demonstrating that the PIP3$^+$ cells are also Insr$^+$, this appears to be extremely likely. These data support two conclusions: first, that the tissues of Δ80 and Δ98 mice consist of an admixture of WT and *Insr* null cells, with few if any cells carrying a heterozygous *Insr* deletion. Second, the findings are consistent with a cell-autonomous mechanism of Insr action, in which the phenotype is directly determined by *Insr* ablation in the target cell, without compensatory mechanisms by which normal cells can send signals to cells lacking Insr.

Growth retardation. At about 30% of normal weight, Δ80 and Δ98 mice are the most severely growth-retarded mice generated by ablating insulin signaling (37). Unlike embryos lacking both IGF1 and IGF2 signaling, which achieve 30% of normal weight (21), the birthweight of Δ80 and Δ98 mice is nearly normal. This observation is consistent with the late onset of the growth-promoting effects of Insr during mouse gestation (4). The likeliest mechanism of the postnatal growth retardation is through increased hepatic Igfbp1, which is known to bind circulating IGF1 and limit its bioavailability (38). Indeed, Igfbp1 overexpression in transgenic mice can cause growth retardation (39), although there are no precedents for such a large increase in Igfbp1 levels as seen in *Insr* mosaics. For example, liver-specific ablation of Insr is not associated with a substantial increase of Igfbp1 levels (40), possibly because, in those experiments, ablation of Insr occurs gradually over the first few weeks of postnatal life (41). Indeed, there is evidence in both humans (42) and rats (43) that Igfbp1 levels are negatively correlated with "free" IGF1, the main determinant of linear growth (44). Our data provide evidence that insulin regulates growth independently of metabolism, and indirectly support the notion that free circulating IGF1 contributes to growth (45).

Lipoatrophy. The lack of WAT could be due either to a failure to differentiate adipocytes or to unrestrained lipolysis, leading to TG depletion. Although the distinction between the two entities is at times difficult and arbitrary, our EM data indicate that mosaic mice possess pre-adipocytes but not mature adipocytes. The failure of most pre-adipocytes to differentiate is consistent with the demonstrated role of Insr in this process (46–48). This phenotype is entirely different from that caused by conditional inactivation of *Insr* in mature adipocytes through the aP2 promoter (49). In that case, adipocytes undergo differentiation but dis-

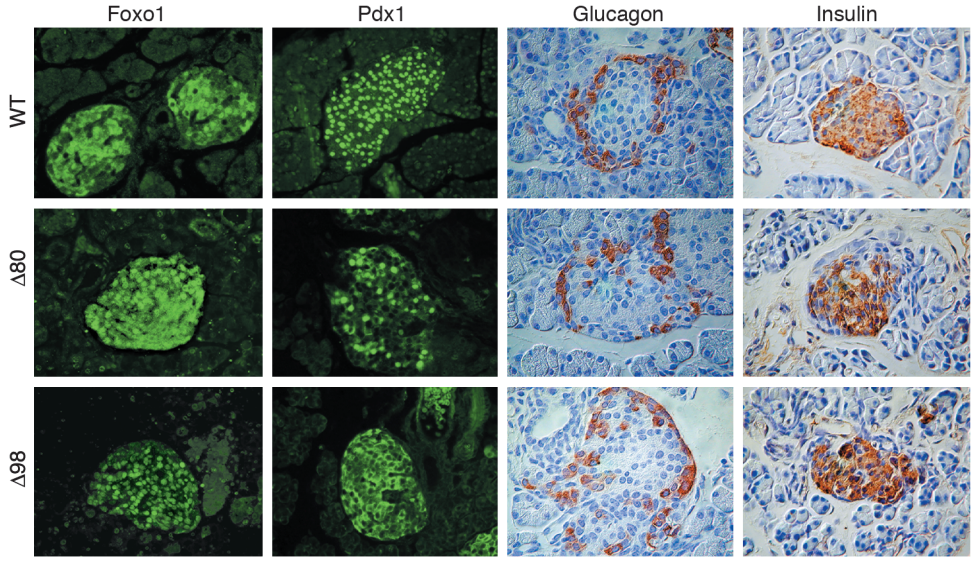

Figure 7
Immunohistochemistry of pancreatic islets. We isolated pancreata from 3-week-old mice and processed them for immunohistochemistry with anti-insulin and anti-glucagon antisera. We used frozen sections for anti-Pdx1 and anti-Foxo1 immunostaining. Note the different intracellular distribution of Pdx1 and Foxo1 between WT and Δ98 mice, and the intermediate pattern in Δ80 mice.

play size heterogeneity. These data, like those mentioned above in mice with liver-specific Insr knockout, underscore the importance of distinguishing between conditional knockouts introduced at different developmental stages in the same cell type (8).

Lipoatrophy is generally associated with profound insulin resistance. However, unlike prior models of lipoatrophy (29, 30), but similar to the double mutants lacking *Irs1* and *Irs3* (50), *Insr* mosaics lack (Δ80 mice) or display modest insulin resistance (Δ98 mice). This dissociation indicates that the development of insulin resistance in lipoatrophy results from the combination of impaired fat storage in adipose tissue and preserved insulin sensitivity in other tissues, primarily the the liver (31). The failure to form an adequate fat mass in *Insr* mosaics appears to be due to reduced expression of key pro-adipogenic genes, since we detected very low levels of *Ucp1*, *Pparγ*, and *Pgc1α* in BAT. This observation is consistent with the role of Insr in adipogenesis (46–48).

β-cell compensation to insulin resistance. Insulin resistance is associated with hyperinsulinemia and leads to β-cell hyperplasia. The lack of compensatory β-cell hyperplasia in *Insr* mosaics could be construed to suggest that insulin signaling is required for this response. These data should be viewed in the context of emerging evidence indicating that insulin signaling regulates various aspects of β-cell function, including proliferation and hormone secretion (51). We have previously shown that the transcription factor Foxo1 is a negative regulator of β-cell proliferation (14). Intriguingly, we now report increased nuclear localization of Foxo1 in β cells of Δ98 mice. These findings are consistent with the view that the lack of β-cell hyperplasia in this model is due to impaired insulin signaling in β cells and/or their progenitors. Although it is possible that the decrease is due to impaired Igf1 signaling, the recent demonstration that ablation of the Igf1 receptor does not affect β-cell proliferation makes this explanation less likely (17, 52). It should be emphasized, however, that the mouse and human models differ in this respect, since children with leprechaunism are more profoundly hyperinsulinemic. Therefore, it remains to be determined whether a similar function can be ascribed to Insr signaling in the human pancreas (6).

Leprechaunism explained? In humans, mutations ablating Insr function give rise to leprechaunism, an invariably fatal syndrome of extreme insulin resistance with growth retardation, lipoatrophy, and hypoglycemia (6). It is unclear why patients with leprechaunism develop hypoglycemia (24). Δ80 mice represent a faithful model of this human syndrome (Table 3). Based on the proposed explanation for the hypoglycemia in Δ80 mice, we suggest that a similar mechanism of impaired insulin action in liver and fat tissue, with preserved insulin sensitivity in muscle tissue, underlies the pathogenesis of hypoglycemia in children with leprechaunism.

Finally, we suggest that future treatment strategies for insulin resistance should strike a balance between improving insulin sensitivity and preventing excessive insulin action by selective targeting of the biologic responses to insulin in different tissues.

Acknowledgments

This work was supported by NIH DK58282 grant and Juvenile Diabetes Research Foundation grant 200-893. T.K. is the recipient of a Juvenile Diabetes Foundation Postdoctoral Fellowship. We thank Youping Liu for skilled technical assistance with immunohistochemistry and members of the Accili laboratory for critical discussion of the data.

1. Saltiel, A.R., and Kahn, C.R. 2001. Insulin signalling and the regulation of glucose and lipid metabolism. *Nature.* **414**:799–806.
2. Kim, J., and Accili, D. 2002. Signalling through IGF-I and insulin receptors: where is the specificity? *Growth Horm. IGF Res.* **12**:84–90.
3. Accili, D., et al. 1996. Early neonatal death in mice homozygous for a null allele of the insulin receptor gene. *Nat. Genet.* **12**:106–109.
4. Louvi, A., Accili, D., and Efstratiadis, A. 1997. Growth-promoting interaction of IGF-II with the insulin receptor during mouse embryonic development. *Dev. Biol.* **189**:33–48.
5. Liu, J.P., Baker, J., Perkins, A.S., Robertson, E.J., and Efstratiadis, A. 1993. Mice carrying null mutations of the genes encoding insulin-like growth factor I (Igf-1) and type 1 IGF receptor (Igf1r). *Cell.* **75**:59–72.
6. Nakae, J., Kido, Y., and Accili, D. 2001. Distinct and overlapping functions of insulin and IGF-I receptors. *Endocr. Rev.* **22**:818–835.
7. Puigserver, P., et al. 2003. Insulin-regulated hepatic gluconeogenesis through FOXO1-PGC-1alpha interaction. *Nature.* **423**:550–555.
8. Kitamura, T., Kahn, C.R., and Accili, D. 2003. Insulin receptor knockout mice. *Ann. Rev. Physiol.* **65**:313–332.
9. Kim, J.K., et al. 2000. Redistribution of substrates to adipose tissue promotes obesity in mice with selective insulin resistance in muscle. *J. Clin. Invest.* **105**:1791–1797.
10. Dietrich, P., Dragatsis, I., Xuan, S., Zeitlin, S., and Efstratiadis, A. 2000. Conditional mutagenesis in mice with heat shock promoter-driven Cre transgenes. *Mamm. Genome.* **11**:196–205.
11. Bruning, J.C., et al. 1998. A muscle-specific insulin receptor knockout exhibits features of the metabolic syndrome of NIDDM without altering glucose tolerance. *Mol. Cell.* **2**:559–569.
12. Kitamura, T., et al. 2001. Preserved pancreatic beta-cell development and function in mice lacking the insulin receptor-related receptor. *Mol. Cell. Biol.* **21**:5624–5630.
13. Chiao, E., et al. 2002. Overgrowth of a mouse model of the Simpson-Golabi-Behmel syndrome is independent of IGF signaling. *Dev. Biol.* **243**:185–206.
14. Nakae, J., et al. 2002. Regulation of insulin action and pancreatic beta-cell function by mutated alleles of the gene encoding forkhead transcription factor Foxo1. *Nat. Genet.* **32**:245–253.
15. Accili, D., et al. 1989. A mutation in the insulin receptor gene that impairs transport of the receptor to the plasma membrane and causes insulin-resistant diabetes. *EMBO J.* **8**:2509–2517.
16. Ooi, G.T., Tseng, L.Y., Tran, M.Q., and Rechler, M.M. 1992. Insulin rapidly decreases insulin-like growth factor-binding protein-1 gene transcription in streptozotocin-diabetic rats. *Mol. Endocrinol.* **6**:2219–2228.
17. Xuan, S., et al. 2002. Defective insulin secretion in pancreatic β cells lacking type 1 IGF receptor. *J. Clin. Invest.* **110**:1011–1019. doi:10.1172/JCI200215267.
18. Sauer, B. 1998. Inducible gene targeting in mice using the Cre/lox system. *Methods.* **14**:381–392.
19. Girard, J., Ferre, P., Pegorier, J.P., and Duee, P.H. 1992. Adaptations of glucose and fatty acid metabolism during perinatal period and suckling-weaning transition. *Physiol. Rev.* **72**:507–562.
20. Lupu, F., Terwilliger, J.D., Lee, K., Segre, G.V., and Efstratiadis, A. 2001. Roles of growth hormone and insulin-like growth factor 1 in mouse postnatal growth. *Dev. Biol.* **229**:141–162.
21. Baker, J., Liu, J.P., Robertson, E.J., and Efstratiadis, A. 1993. Role of insulin-like growth factors in embryonic and postnatal growth. *Cell.* **75**:73–82.
22. Barnard, T. 1969. The ultrastructural differentiation of brown adipose tissue in the rat. *J. Ultrastruct. Res.* **29**:311–322.
23. Tsukiyama-Kohara, K., et al. 2001. Adipose tissue reduction in mice lacking the translational inhibitor 4E- BP1. *Nat. Med.* **7**:1128–1132.
24. Taylor, S.I. 1992. Lilly Lecture: molecular mechanisms of insulin resistance. Lessons from patients with mutations in the insulin-receptor gene. *Diabetes.* **41**:1473–1490.
25. Guillam, M.T., Burcelin, R., and Thorens, B. 1998. Normal hepatic glucose production in the absence of GLUT2 reveals an alternative path-

way for glucose release from hepatocytes. *Proc. Natl. Acad. Sci. U. S. A.* **95**:12317–12321.
26. Rausa, F.M., et al. 2000. Elevated levels of hepatocyte nuclear factor 3beta in mouse hepatocytes influence expression of genes involved in bile acid and glucose homeostasis. *Mol. Cell. Biol.* **20**:8264–8282.
27. Daitoku, H., Yamagata, K., Matsuzaki, H., Hatta, M., and Fukamizu, A. 2003. Regulation of PGC-1 promoter activity by protein kinase B and the forkhead transcription factor FKHR. *Diabetes.* **52**:642–649.
28. Yoon, J.C., et al. 2001. Control of hepatic gluconeogenesis through the transcriptional coactivator PGC-1. *Nature.* **413**:131–138.
29. Moitra, J., et al. 1998. Life without white fat: a transgenic mouse. *Genes Dev.* **12**:3168–3181.
30. Shimomura, I., et al. 1998. Insulin resistance and diabetes mellitus in transgenic mice expressing nuclear SREBP-1c in adipose tissue: model for congenital generalized lipodystrophy. *Genes Dev.* **12**:3182–3194.
31. Shimomura, I., et al. 2000. Decreased IRS-2 and increased SREBP-1c lead to mixed insulin resistance and sensitivity in livers of lipodystrophic and ob/ob mice. *Mol. Cell.* **6**:77–86.
32. Chakravarty, K., et al. 2001. Sterol regulatory element-binding protein-1c mimics the negative effect of insulin on phosphoenolpyruvate carboxykinase (GTP) gene transcription. *J. Biol. Chem.* **276**:34816–34823.
33. Fleischmann, M., and Iynedjian, P.B. 2000. Regulation of sterol regulatory-element binding protein 1 gene expression in liver: role of insulin and protein kinase B/cAkt. *Biochem. J.* **349**:13–17.
34. Slack, J.M. 1995. Developmental biology of the pancreas. *Development.* **121**:1569–1580.
35. Macfarlane, W.M., et al. 1999. Glucose stimulates translocation of the homeodomain transcription factor PDX1 from the cytoplasm to the nucleus in pancreatic beta-cells. *J. Biol. Chem.* **274**:1011–1016.
36. Kitamura, T., et al. 2002. The forkhead transcription factor Foxo1 links insulin signaling to *Pdx1* regulation of pancreatic β cell growth. *J. Clin. Invest.* **110**:1839–1847. doi:10.1172/JCI200216857.
37. Efstratiadis, A. 1998. Genetics of mouse growth. *Int. J. Dev. Biol.* **42**:955–976.
38. Clemmons, D.R. 1998. Role of insulin-like growth factor binding proteins in controlling IGF actions. *Mol. Cell. Endocrinol.* **140**:19–24.
39. Schneider, M.R., Lahm, H., Wu, M., Hoeflich, A., and Wolf, E. 2000. Transgenic mouse models for studying the functions of insulin-like growth factor-binding proteins. *FASEB J.* **14**:629–640.
40. Michael, M.D., et al. 2000. Loss of insulin signaling in hepatocytes leads to severe insulin resistance and progressive hepatic dysfunction. *Mol. Cell.* **6**:87–97.
41. Postic, C., and Magnuson, M.A. 2000. DNA excision in liver by an albumin-Cre transgene occurs progressively with age. *Genesis.* **26**:149–150.
42. Frystyk, J., Grofte, T., Skjaerbaek, C., and Orskov, H. 1997. The effect of oral glucose on serum free insulin-like growth factor-I and -II in health adults. *J. Clin. Endocrinol. Metab.* **82**:3124–3127.
43. Frystyk, J., et al. 1998. Developmental changes in serum levels of free and total insulin-like growth factor I (IGF-I), IGF-binding protein-1 and -3, and the acid-labile subunit in rats. *Endocrinology.* **139**:4286–4292.
44. Yakar, S., et al. 2002. Circulating levels of IGF-1 directly regulate bone growth and density. *J. Clin. Invest.* **110**:771–781. doi:10.1172/JCI200215463.
45. D'Ercole, A.J., and Calikoglu, A.S. 2001. Editorial review: the case of local versus endocrine IGF-I actions: the jury is still out. *Growth Horm. IGF Res.* **11**:261–265.
46. Accili, D., and Taylor, S.I. 1991. Targeted inactivation of the insulin receptor gene in mouse 3T3-L1 fibroblasts via homologous recombination. *Proc. Natl. Acad. Sci. U. S. A.* **88**:4708–4712.
47. Entingh, A.J., Taniguchi, C.M., and Kahn, C.R. 2003. Bi-directional regulation of brown fat adipogenesis by the insulin receptor. *J. Biol. Chem.* **278**:33377–33383.
48. Nakae, J., et al. 2003. The forkhead transcription factor Foxo1 regulates adipocyte differentiation. *Dev. Cell.* **4**:119–129.
49. Bluher, M., et al. 2002. Adipose tissue selective insulin receptor knockout protects against obesity and obesity-related glucose intolerance. *Dev. Cell.* **3**:25–38.
50. Laustsen, P.G., et al. 2002. Lipoatrophic diabetes in Irs1(–/–)/Irs3(–/–) double knockout mice. *Genes. Dev.* **16**:3213–3222.
51. Accili, D. 2001. A kinase in the life of the β cell. *J. Clin. Invest.* **108**:1575–1576. doi:10.1172/JCI200114454.
52. Kulkarni, R.N., et al. 2002. Beta-cell-specific deletion of the Igf1 receptor leads to hyperinsulinemia and glucose intolerance but does not alter beta-cell mass. *Nat. Genet.* **31**:111–115.